Research Article

Journal of Environmental Nanotechnology

Green Solvent-mediated Solution Combustion Synthesis of Photocatalytic Active Copper-doped Zinc Oxide Nanoparticles and their Antimicrobial Activity Study

P. Vinisha Valsaraj[1*], P. Ashna[2], Anagha Rajan[2] and Sreshma Rajan[2]

[1]PG and Research Department of Chemistry, Sree Narayana College, Kannur, Kannur University, KL, India

[2]Department of Physics, Sree Narayana College, Kannur, Kannur University, KL, India

Received: 16.09.2024 Accepted: 22.11.2024 Published: 30.12.2024

*vinipunep@gmail.com

ABSTRACT

Environmental concerns over water pollution, particularly from chemical and biological sources, have become increasingly pressing in contemporary society. This study investigates the effectiveness of solution combustion synthesized pure and copper-doped zinc oxide nanoparticles in photocatalytically degrading dye pollutants focusing on methylene blue. Using a green solvent solution combustion process, copper-doped zinc oxide nanoparticles were prepared and tested for their ability to degrade methylene blue dye. Parameters influencing the photodegradation efficiency including catalyst concentration, pH levels, and dye concentration were systematically evaluated. Results indicate that the photocatalytic degradation of methylene blue dye increases with irradiation time, achieving up to 94% degradation in just three hours. The nanoparticles were characterized using XRD, UV-visible diffuse reflectance spectroscopy, Raman spectroscopy, and SEM. The antimicrobial activity of synthesized nanoparticles was evaluated against gram-positive and gram-negative bacteria. The copper-doped zinc oxide exhibited significant antimicrobial activity, with a zone of inhibition measuring 12 mm and 17 mm against E. coli and Staphylococcus aureus, respectively. By leveraging their multifunctional properties, these nanoparticles not only contribute to improving public health through their microbial properties but also play a crucial role in environmental remediation by breaking down harmful organic compounds. Thus, they represent a promising innovation in medicine and environmental science, offering a sustainable solution to mitigate pollution caused by organic dye.

Keywords: Green solvent; Solution combustion synthesis; Doping; Photocatalytic activity; Antimicrobial activity.

1. INTRODUCTION

Large-scale textile production uses synthetic dyes with long-lasting chemical and physical properties. The use of these dyes and the disposal of the dye waste from these enterprises pose significant risks to the environment (Ding *et al.* 2014; Qiu B *et al.* 2014; Qi *et al.* 2014; Xing *et al.* 2014). Ultrafiltration, reverse osmosis, ion exchange, adsorption, and photocatalytic degradation are examples of conventional techniques for eliminating these colors from aqueous solutions. These techniques, nevertheless, frequently fall short of totally degrading the organic contaminants. Photocatalytic degradation is an important and efficient technique for removing this dye from an aqueous solution. Due to the exceptional photocatalytic, electrical, and photochemical qualities at ambient temperature, semiconductor metal oxides like wurtzite zinc oxide (ZnO) - a II-VI semiconducting oxide present a viable option for the photodegradation of dyes (Wang *et al.* 2018; Zhou *et al.* 2014; Zhang *et al.* 2014; Mo *et al.* 2014; Banu Bahşi *et al.* 2007; Ozgur *et al.* 2005). Despite this, ZnO has a broad bandgap and absorbs most wavelengths in the UV (>380 nm) area, which makes up only 5% of the solar spectrum. The high rate of recombination presents another difficulty. Many techniques have been developed to improve the efficiency of ZnO in charge carrier separation and light absorption. These techniques consist of surface modification, morphological optimization, hybrid structure creation, and doping with cationic or anionic components. Doping with transition metals has attracted a lot of interest among them (Hyun *et al.* 2004; He *et al.* 2005; Deka *et al.* 2007; Saleh *et al.* 2014; Manju Kumari *et al.* 2022). By producing flaws in the host lattice, this method expands the bandgap's energy levels. This means that the optical and physical characteristics of ZnO can be changed by adding transition metal ions, which is important for optical applications.

The potential of nanoparticles (NPs) as a viable substitute for conventional antimicrobial medications in the treatment of infectious diseases is being investigated more and more. Among them, plant extracts have been used in the synthesis of metal and metal oxide nanoparticles, which have shown strong antibacterial effects against a range of bacterial species. Studies show

that doping methods can improve these nanoparticles' antibacterial activity even more. One example of a nanoparticle with antibacterial action is ZnO, which is mainly attributable to the generation of reactive oxygen species (ROS) and the release of zinc ions. Dopants, including the transition metals Fe, Cu, Mg, and Mn, among others, can improve the optical and antibacterial characteristics of ZnO NP. Cu is an important metal for doping since it is a member of the transition metal family, has a high electrical conductivity, and almost has the same ionic radius as zinc oxide. Cu doping into the ZnO matrix can improve its physical, chemical, optical, and antibacterial properties, according to literature studies.

Chemical and physical methods are employed in the nanoscale material synthesis of ZnO nanoparticles (ZnO NPs). Recently, there has been a lot of focus on reducing the primary drawback of the physical and chemical processes used to manufacture ZnO nanoparticles, which include their high energy consumption and substantial use of toxic chemicals. Solution Combustion Synthesis (SCS) is a good technique that is well-known for its ease of use, energy efficiency, and time efficiency in enhancing dopant distribution throughout the combustion process (Deganello *et al.* 2018; Shikha *et al.* 2024). In SCS, precursors are broken down in the presence of a fuel that serves as a reducing agent. This process results in the creation of sol and gel after heat-assisted solvent removal. The materials ignite and release gases when they reach the ignition temperature. Traditional SCS techniques, however, have several drawbacks, such as the use of hazardous chemicals, and poisonous byproducts. Consequently, there has been an increase in interest in environmentally benign methods of synthesizing nanoparticles. The environment-friendly, low-cost, and less hazardous green approaches make them appealing. Green solvents have been added to SCS as fuel, which has improved the method considerably and more environment-friendly while offering a higher progressive response rate than traditional chemicals.

This study adopts a green solvent-mediated solution combustion approach to synthesize zinc oxide nanoparticles (ZnO NPs) and ZnO NPs doped with copper. With this technique, dangerous chemicals and physical procedures are avoided; only a small amount of Moringa oleifera leaf extract is needed. ZnO and Cu-doped ZnO NPs are synthesized at varying dopant concentrations of 1% and 2% by weight for the investigation. Techniques including Raman Spectroscopy, UV-Visible Diffuse Reflectance Spectroscopy (DRS), Scanning Electron Microscopy (SEM), and X-ray Diffraction (XRD) are used to analyze the physical and optical properties of the produced nanoparticles. Using methylene blue (MB) dye as the organic pollutant, the photocatalytic activities of the samples are assessed in the presence of visible light. Additionally, using the Agar well diffusion method, the antibacterial effectiveness of produced materials against gram-positive and gram-negative bacteria was examined.

2. MATERIALS AND METHODS

2.1 Materials

All of the compounds, which included zinc nitrate hexahydrate (Zn $(NO_3)_2.6H_2O$), (Merck); copper (II) nitrate trihydrate (Cu $(NO_3)_2.3H_2O$), (Merck), Methylene Blue (MB) dye (Merck) were of analytical grade and were employed without any additional purification. Double-distilled water was used to prepare each solution.

2.2 Methods

Moringa oleifera was collected for this experiment from Sree Narayana College, Kannur, India and after being cleaned with distilled water, 500 g of it was boiled in 500 ml distilled water for an hour at 100 °C. Finally, the extract was filtrated and preserved for further use.

2.2.1 Synthesis of Zinc Oxide Nanoparticles (ZnO NPs)

ZnO nanoparticles were synthesized by mixing newly prepared 40 ml of Moringa oleifera leaf extract, which served as fuel, with 0.1 M zinc nitrate in a small amount of distilled water. A magnetic stirrer was used to thoroughly agitate the liquid for 30 minutes. Following homogenization, the precursor solution was transferred to a dish and heated to a temperature where it gelled. An ignition reaction was then created, propagating spontaneously, and dried powder was produced by heating the mixture to 250 °C on a hot plate. Ceramic crucibles were used to gather this powder. Optimization was utilized to determine the mass of zinc nitrate, the extract volume, and the calcination temperatures. Every product was calcined in a muffle furnace for two hours at 800 °C.

2.2.2 Synthesis of Copper-doped Zinc Oxide Nanoparticles (Cu-ZnO NPs)

The same procedure used for the synthesis of ZnO NPs was adopted. For the synthesis of Cu-doped ZnO NPs, along with zinc nitrate precursor, copper nitrate solution corresponding to 1% doping and 2% doping was added separately. Here also green solvent is used as fuel for solution combustion synthesis. The mass of zinc nitrate and copper nitrate, the volume of extract, and the calcination temperatures used were obtained by optimization. All the products were calcinated for 2 hours in a muffle furnace at 800 °C and stored for characterization.

2.3 Characterizations

The characteristic X-ray diffraction patterns of prepared nanostructures were recorded using Powder XRD (Rigaku Miniflex 600) using CuKλ radiation (λ= 1.54060 Å) for measuring the crystalline nature of atoms in the material. The diffractograms were recorded in the range of 2θ from 20° to 80° at a scanning speed of 2 °/min at room temperature. JEOL Model JSM - 6390LV for scanning electron microscopic analysis, and JEOL Model JED – 2300 for energy dispersive spectrometric (EDS) measurements were used for morphological characterizations. To probe the elastic scattering processes in these materials, micro-Raman spectroscopy was performed employing WITec alpha300RA (WITec GmbH, Ulm, Germany) AFM, SNOM & RAMAN combined system. UV-visible Spectrophotometer model JASCO V660 with integrated sphere attachment was used for spectrophotometric measurements.

2.4 Photocatalytic Activity Study

To study the photocatalytic degradation of methylene blue, 100 mg of photocatalyst (ZnO, 1% Cu-doped ZnO) was dispersed in 50 ml of 10 ppm aqueous MB solution. Then, the reaction mixture was stirred for 15 min at room temperature under dark conditions to attain adsorption-desorption equilibrium between photocatalyst and MB. Then, the reaction mixture was placed under visible light irradiation. 2 ml of MB solution was withdrawn every 60 min to observe the degradation process by taking absorption spectra using a UV-visible spectrophotometer. The absorbance of MB before and after irradiation at regular intervals of time was used to calculate the percentage degradation efficiency (%D) of photocatalysts using the equation (Ravichandran *et al.* 2014),

$$\%D = (A_0 - A_t/A_0) \times 100 \quad \ldots\ldots (1)$$

where, A_0 and A_t are absorbance recorded initially and absorbance recorded at different times, respectively.

2.5 Antimicrobial Activity Study

For the investigation of antimicrobial activity, the Agar well diffusion method was used. Bacterial cultures of Staphylococcus aureus and E. coli were seeded into petriplates containing 20 ml of Muller Hinton Agar Medium (growth of culture controlled according to McFarland Standard, 0.5%). Using a well cutter, wells of roughly 10 mm were bored, and samples in varying concentrations of 250 µg/ml, 500 µg/ml, and 1000 µg/ml were added. After that, the plates were incubated for 24 hours at 37 °C. The diameter of the inhibition zone that developed around the well served as a proxy for the antibacterial activity (NCCLS, 1993). The positive control in this case was streptomycin.

3. RESULTS AND DISCUSSION

3.1 XRD Analysis

The strong diffracted intensity of X-rays confirmed that both pure and Cu-doped ZnO NPs exhibited a good crystalline nature. XRD patterns of Cu-doped ZnO NPs were the same as those of pure ZnO NPs, and they were verified by the JCPDS card (36-1451) and reference code (01-097-0207), which indexed the samples to the hexagonal wurtzite phase (Richa *et al.* 2018; Geetha *et al.* 2010). From Fig. 1, at 2θ angles of 31.84°, 34.52°, 36.21°, 47.63°, 56.71°, 62.96°, 68.13°, and 69.18° were detected which corresponded to the Miller indices (1 0 0), (0 0 2), (1 0 1), (1 0 2), (1 1 0), (1 0 3), (1 1 2), and (2 0 1) respectively. The Debye-Scherrer formula,

$$D = (0.94\lambda)/ (\beta \cos \theta) \ldots. (2)$$

where, D is the crystallite size, K is the Scherrer constant, λ is the X-ray wavelength, β is the full width at half maximum (FWHM), and Θ is the Bragg's angle, was used to get the average crystallite size, which was 42 nm for pure ZnO NPs and 42 nm and 37 nm for 1% and 2% Cu-doped ZnO NPs, respectively (Wibowo *et al.* 2013).

The lattice constant for hexagonal wurtzite ZnO and copper-doped zinc oxide NPs were estimated from the equation (Nimbalkar *et al.* 2017),

$$d_{hkl} = \frac{1}{\sqrt{\frac{4}{3}\left(\frac{h^2 + k^2 + hk}{a^2}\right) + \frac{l^2}{c^2}}} \quad \ldots.. (3)$$

where, a and b are the lattice constant, h, k, and l are the Miller indices and d is the interplanar spacing. The interplanar spacing can be calculated from Bragg's law: $2d\sin\Theta = n\lambda$ (Mhamdi *et al.* 2014). In addition, the microstrain (Ɛ) of samples was calculated by the equation,

$$\text{Micro strain } (\varepsilon) = \frac{\beta \cos\Theta}{4} \quad \ldots\ldots (4)$$

where, Ɛ is the microstrain, β is the full width at the half maximum (FWHM) and Θ is the Bragg's angle. The crystalline size, lattice parameters, and microstrain are presented in Table 1.

For pure ZnO NPs, the lattice constants were a = 0.3250 nm and c = 0.5210 nm. The lattice constants for 1 % Cu-doped ZnO are a = 0.3249 nm and c = 0.5204 nm and for 2% Cu-doped ZnO are a = 0.3230 and c = 0.5180. 2%. Cu doping caused a minor shift in peak positions while increasing the copper content, which showed that

Cu ions were substituted and incorporated into the ZnO lattice. The XRD spectra did not show any secondary phases, such as Cu_2O, CuO, or other metallic Cu or Zn phases. Since Cu (0.073 nm) and Zn (0.074 nm) have similar ionic radii, it is most likely because of this that Cu ions may more easily be incorporated into the ZnO lattice, explaining the absence of copper oxide peaks. The consistent XRD patterns before and after doping show that doping ZnO with Cu ions does not appreciably alter the phase structure of the material. According to this investigation, the crystalline and the structural integrity of pure ZnO were retained in Cu-doped ZnO which is due to the phytochemicals in the green solvent acting as fuels in solution combustion synthesis, functioning as capping agents (Singhal *et al.* 2015).

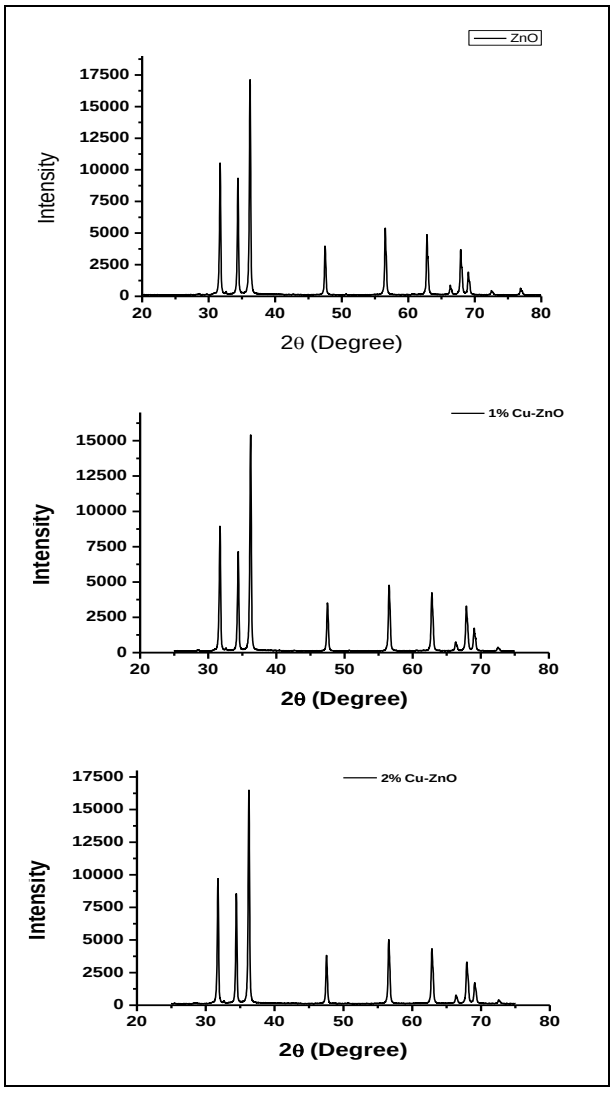

Fig. 1: XRD Patterns of ZnO NPs and 1% & 2% Cu-doped ZnO NPs

The introduction of Cu into the Zn lattice induced a compressive strain within the structure, shifting the peak locations of the X-ray diffractograms towards higher diffraction angles. Additionally, there was a modest decrease in the cell volume for the doped samples. As the doping concentration increased, the average crystallite size decreased. This phenomenon can be attributed to the distortion of the host material's crystal lattice by impurities, which slows down the nucleation and growth rates. This behavior is explained by the Zener pinning theory, which describes the movement of grain boundaries across the edges of the grains. According to this theory, the edges of the crystallites exert a force on the moving boundaries, and these boundaries may become pinned if Cu ions replace Zn atoms. Since the obstructing force is greater than the driving force for grain growth (Eg), crystallite growth is hindered. Furthermore, the doping of Cu in ZnO can lead to charge imbalance and crystal defects around the dopants, further altering the ZnO crystal lattice and causing the crystallite size to decrease as the doping concentration increases. Reduced doping concentrations cause fewer contaminants to enter the host material, which lessens the amount of crystal lattice distortion. This may aid in preserving the material's inherent qualities, which will facilitate research into its basic optical characteristics. Consequently, further study was carried out on 1% copper-doped zinc oxide NPs.

3.2 Raman Analysis

The impact of copper doping on ZnO nanostructures was examined using room-temperature micro-Raman spectra for each sample. A comparison of the Cu-doped ZnO micro-Raman spectrum with the undoped ZnO spectrum is shown in Fig. 2. Both spectra show that the pure and doped ZnO material has a good wurtzite structure (Thilagavathi *et al.* 2014). The spectra reveal peaks at 334 cm^{-1}, 387 cm^{-1}, 437 cm^{-1} and 574 cm^{-1} corresponding to E_{2H} - E_{2L}, A_1(TO), E_{2H} and A_1(LO)/E_1(LO) modes of ZnO, respectively. The E_{2L} in zinc oxide is associated with the vibration of the heavy Zn sub-lattice and E_{2H} mode is characteristic of the wurtzite phase. The peak at 437 cm^{-1} is the characteristic E_{2H} peak of ZnO and is mainly due to the vibration of oxygen atoms which verifies the wurtzite hexagonal structure of both samples (Silambarasan *et al.* 2015; Lupan *et al.* 2010). Effect of Cu-doping on the E_{2H} mode of ZnO can visible while its intensity decreases than corresponding ZnO (Davis *et al.* 1970; Taut *et al.* 1966). The nearly similar wave vibration positions and wave intensity of the Raman spectra show no noticeable variation between the samples. This could be due to the relatively low (≤7 mol. %) Cu^{2+} doping level in the ZnO sample. Interestingly, the spectra of the Cu-doped ZnO nanostructures show no Raman peaks corresponding to CuO or Cu_2O, indicating the absence of secondary phases in the copper-doped samples, which is consistent with the XRD data. This offers more proof for the extremely small (≤7 mol.%) amount of Cu^{2+} doped into the ZnO lattice. The manufacture of zinc oxide with 1 wt. % copper

doping using the green solvent-mediated solution combustion approach resulted in less stress and strain, as evidenced by the lack of shifts and broadening of Raman peaks in comparison with the available literature data.

Table 1: Calculated values of FWHM, average crystallite size, lattice parameters, cell volume, and interplanar distance and microstrain for ZnO, 1% and 2% Cu-ZnO NPs

Data	2Θ (°)	hkl	d_{hkl}(A^0)	Lattice parameters (A^0)	V (A^0)^3	Crystal size, D (nm)	Bond length L(A^0)	Micro strain, ϵ
ZnO	31.75	100	2.818	a =3.25	47.65	42.12	0.6304	0.857x10^{-3}
	34.39	002	2.605	c=5.21				
1% Cu-ZnO	31.77	100	2.81	a=3.249	47.56	42	0.62	0.87 x 10^{-3}
	34.44	002	2.6	c=5.203				
2% Cu-ZnO	31.91	100	2.80	a=3.23	46.8	37.14	0.623	0.956 x 10^{-3}
	34.58	002	2.59	c=5.18				

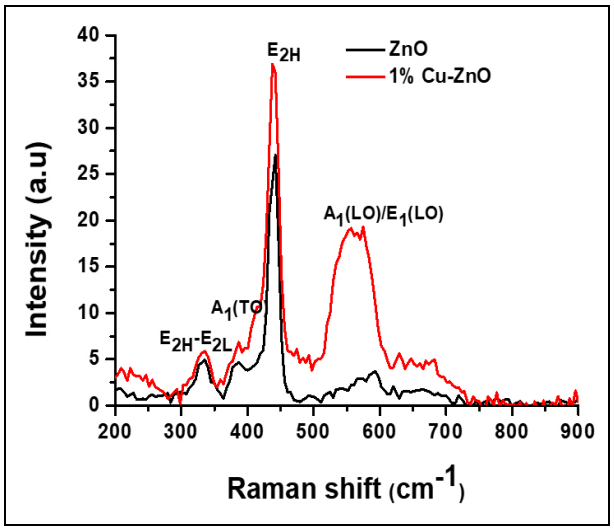

Fig. 2: Raman Spectra of ZnO and 1% Cu-ZnO

3.3 Optical Property Study

Fig. 3 displays the room temperature absorption spectra of the Cu-doped and pure ZnO NPs. It is clear from the image that ZnO shows discernible absorption in the 255–367 nm range whereas in the case of Cu-ZnO absorption is in the 255-387 nm range. Using Taut's plot, photon energy (hν) versus $(\alpha h\nu)^2$, where α is the optical absorption coefficient close to the fundamental absorption edge, the band gap energies of the produced samples were determined (Mott *et al.* 1971; Muthukumaran *et al.* 2012). The band gap of the sample doped with 1% Cu is 2.7 eV, while the band gap of the pure ZnO is 3.1 eV, as shown by Taut's plot (Fig. 4). Both values are less than the band gap of bulk ZnO, revealing that doping lowers the bandgap of ZnO nanostructures. Electronegativity of copper (1.9) is higher than that of ZnO (1.6), resulting in a chemical effect that lowers the band gap energy in the host ZnO crystal; also, the sp-d exchange interactions between the d orbitals of the Cu dopant and the sp orbitals of the host ZnO cause a positive correction in the valence band and a negative correction in the conduction band, causing overall band narrowing (Diouri *et al.* 1985; Menon *et al.* 2017). The absorbance peak shifts slightly red from 360 nm to 380 nm when ZnO NPs are doped with Cu which corresponds to the strong surface plasmon resonance, suggesting a narrowing of the band gap and the shift in the surface plasmon resonance is due to the interaction of two different metal ions present in the copper-doped zinc oxide nanoparticles (Labhane *et al.* 2015). The absorption characteristics of Cu-doped ZnO nanoparticles can be influenced by the production process. In particular, ZnO nanoparticles produced by the solid-state method exhibit a blue shift, suggesting that the optical characteristics of the nanoparticles can be influenced by various reaction techniques. The text focuses on how Cu doping affects the optical and electrical characteristics of ZnO nanoparticles, highlighting how crucial the synthesis process and the doping element are in defining these characteristics.

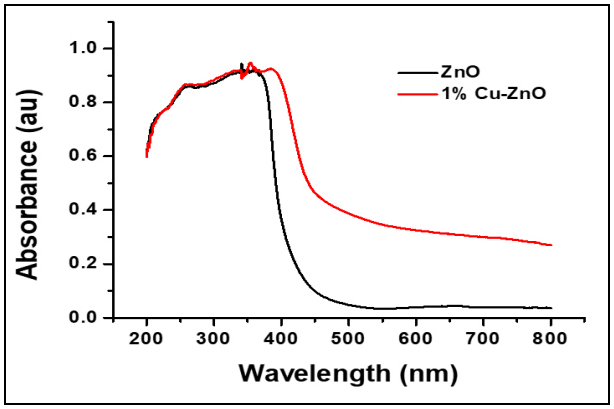

Fig. 3: UV-visible Diffuse Spectra of ZnO NPs And 1% Cu-ZnO NPs

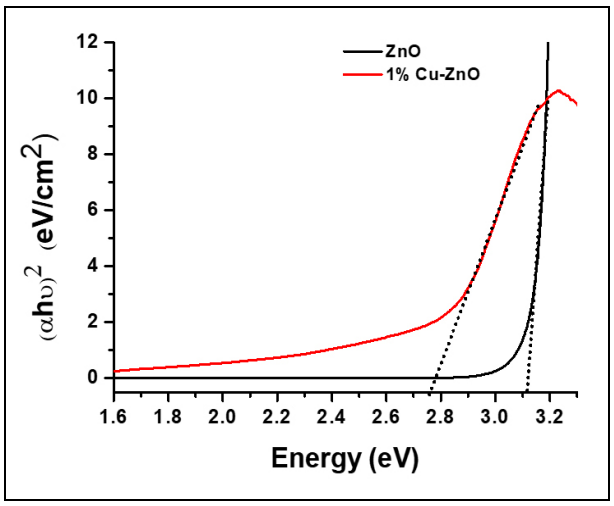

Fig. 4: Taut Plot of ZnO NPs and 1% Cu-ZnO NPs

Table 2: The Elemental Percentage Compositions of ZnO and 1% Cu-ZnO NPs from EDX

Sample	Elements	Weight %	Atomic %
ZnO	O	15.46	42.76
	Zn	84.54	57.24
	Total	100	100
1% Cu-ZnO	O	15.52	42.87
	Cu	1.06	0.84
	Zn	83.42	56.29
	Total	100	100

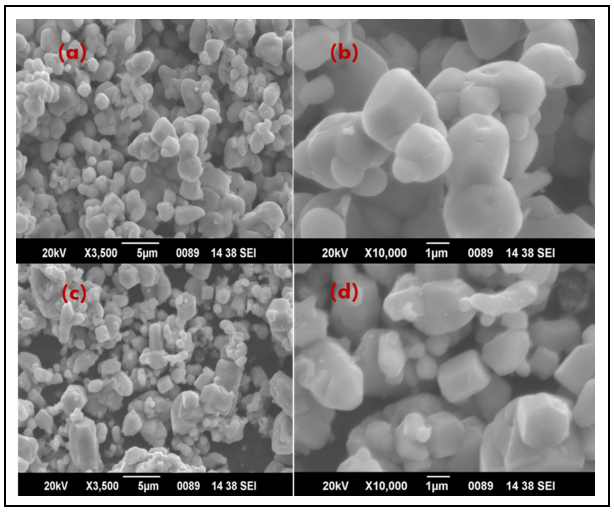

Fig. 5: Scanning Electron Micrographs of: (a & b) ZnO NPs And 1% Cu-ZnO NPs and (c & d) at Different Magnifications

3.4 SEM-EDX Analysis

SEM was used to observe the generated samples' grain size and crystal shape. Fig. 5 shows the SEM pictures of pure and copper-doped ZnO NPs. The ZnO nanoparticles and 1% Cu-ZnO NPs have a spherical morphology, as seen by the SEM micrograph, and they create a structure that resembles tiny balls grouped in a box-like configuration. This spherical shape was further highlighted by the nanoclusters seen on the surface of these particles. These nanoparticles were produced using a green solvent-mediated solution combustion process, yielding nanometer-scale particles that are strongly agglomerated and well-dispersed, exhibiting a nearly well-defined crystalline character.

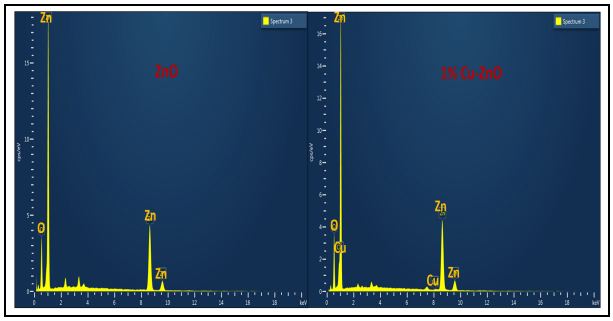

Fig. 6: EDX Analysis of ZnO NPs and 1% Cu-ZnO NPs

The elemental composition of the produced samples was examined using Energy-dispersive X-ray (EDX) analysis, which also demonstrated the successful doping and synthesis of ZnO NPs. Fig. 6 displays the EDX signals and each sample's percentage makeup. The elemental percentage composition of all the samples is presented in Table 2. Sharp signals for oxygen and zinc were detected for un-doped ZnO NPs, confirming the production of ZnO NPs. Along with zinc and oxygen, copper signals were also detected for Cu-doped samples, which indicated successful Cu doping.

3.5 Photocatalytic Activity Study

Under visible light, the photocatalytic activity of the resulting pure and Cu-doped ZnO NPs was determined in comparison to the MB dye degradation. By utilizing the usual absorption peak of MB dye at 670 nm, the degradation process was observed. The absorption spectra of an aqueous MB solution with ZnO and Cu-doped ZnO NPs present at different time intervals are shown in Fig. 7. The findings demonstrated that when the visible light irradiation period increased, the absorbance of MB dye was reduced for both samples and absorbance of methylene blue is higher in the case of ZnO compared with Cu-doped ZnO. In particular, as exposure times increased, the MB peak strength decreased, suggesting that the MB dye was degrading in the presence of the nanoparticles. When light is applied to Cu-doped ZnO, electrons are excited from the valence band to the conduction band, forming electron-hole pairs. Hydroxyl radicals (•OH) are created when water molecules interact with the holes in the valence band (positive charge). These extremely reactive oxidizing agents, known as radicals, can decolorize organic dye molecules by breaking them down. $O_2^{\bullet-}$, or superoxide

anion radicals, can be created in a solution when dissolved oxygen (O_2) is reduced by photoexcited electrons in the conduction band (Ahmad *et al.* 2013). Strong oxidizers, these radicals can further break down organic dye molecules in close proximity to the surface of the catalyst. Generally, the highly efficient degradation of organic dyes is caused by the combined action of superoxide anion and hydroxyl radicals produced during the photoexcitation of Cu-doped ZnO than the pure ZnO.

A study on the impact of pH in dye degradation is crucial since it influences many factors, such as the catalyst's charge, the positions of the valence and conduction bands, and the generation of hydroxyl radicals (Pandian *et al.* 2018; Mahajan *et al.* 2019). These variables affect the catalyst's effectiveness as well as the properties of textile wastes. The methylene blue (MB) dye was subjected to a 180-minute degradation process using Cu-doped ZnO NPs at pH values of 4, 6, 8, and 10 while maintaining a constant dye concentration of 10 ppm. pH of the solution was regulated with the help of HNO_3 and NaOH. A strong association between the pH level and dye degradation efficiency was observed as illustrated in Fig. 8 a. About 65% of the color broke down at pH 4. The rate of degradation increased with increasing pH, and it reached 80%, 85%, and 90% for pH levels 6, 8, and 10, respectively. This implies that higher pH values accelerate the rate of breakdown, most likely because they cause more hydroxyl radicals to develop. The pattern of variation for pH was the same in both samples.

The study investigates the impact of varying catalyst concentrations on the photodegradation of Methylene Blue (MB) in an aqueous solution for both samples which shows that the degradation rate of MB increases as catalyst concentrations rise (Fig. 8 b). The increase in active sites can be considered as the cause of this acceleration since it increases the formation of hydroxyl and superoxide radicals, which are responsible for dye degradation. The inverse link between dye concentration and decomposition efficiency was highlighted by the observed difference in photodegradation rates caused by varying MB concentrations. Fig. 8 c shows that the degradation rate reduces with increasing MB concentration. The decrease in the rate of degradation is probably the result of dye molecules on the Cu-doped ZnO surface absorbing UV radiation rather than catalyst molecules. The dye molecules decrease the production of hydroxyl radicals by blocking the photocatalysts' active sites (Premanathan *et al.* 2013). Following the initial cycle of dye breakdown by the samples, distilled water was used to properly wash the samples to determine their recycling potential. The identical dye degradation test was conducted for three hours using a 10 ppm MB solution; UV-visible DRS was used to record the absorption spectra. Once again, the experiment was carried out. The result aligns with the great potential for sample recycling that has been established, as seen in Fig. 9.

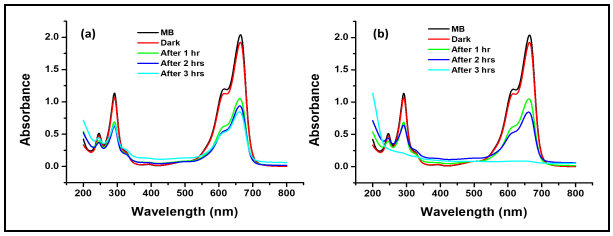

Fig. 7: MB Dye Degradation under Sunlight Irradiation at different time intervals in the presence of (a) ZnO NPs and (b) 1% Cu-ZnO NPs

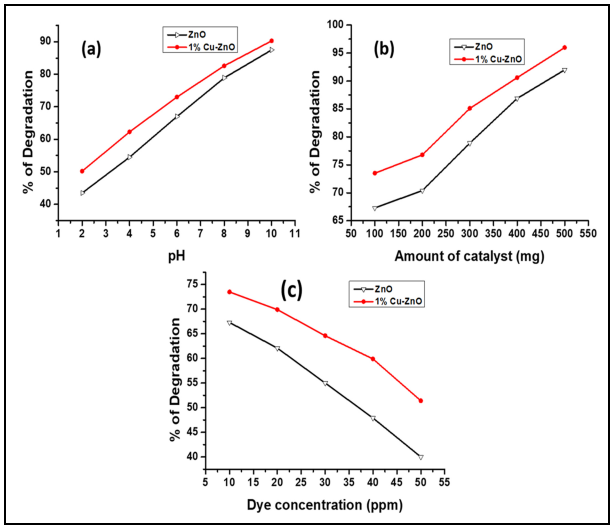

Fig. 8: Dye Degradation Percentage of ZnO and 1% Cu-ZnO NPs: (a) Effect of pH, (b) Effect of Amount of Catalyst, and (c) Effect of Concentration of MB

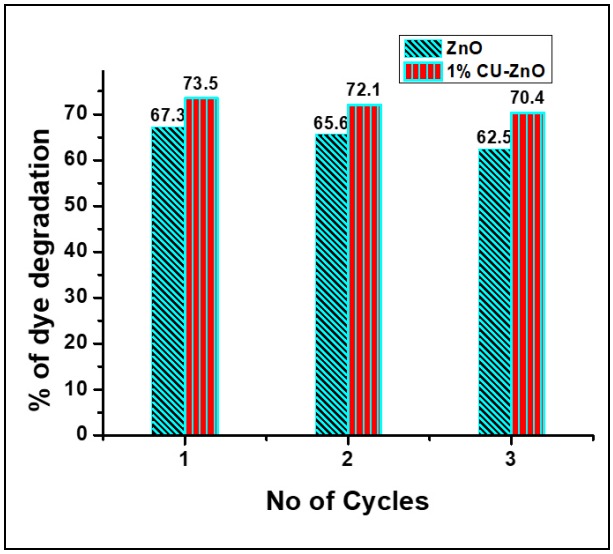

Fig. 9: Dye Degradation Percentage for different cycles of ZnO and 1% Cu-ZnO NPs

3.6 Antimicrobial Activity Study

The antibacterial activity of produced un-doped and Cu-doped ZnO NPs against gram-positive (S. aureus) and gram-negative (E. coli) bacteria was investigated using the Disc diffusion method. Fig. 10 shows the zone of inhibition (ZOI) surrounding the disc, and Table 3 provides the measured values of inhibition. For this investigation, streptomycin is employed as the primary antibiotic. It has a ZOI of 27 mm against Staphylococcus aureus for 100 µg and a ZOI of 32 mm against E. coli for 100 µg. The results show that Cu-doped ZnO NPs limit the development of all tested microorganisms more effectively than ZnO NPs across all tested doses. Compared to gram-negative bacteria, it was found that the gram-positive bacteria are more vulnerable to Cu-doped ZnO NPs. ZOI for ZnO NPs was nil for gram-positive S. aureus and 12 mm for gram-negative E. coli. The ZOI for Cu-doped ZnO NPs was 17 mm for gram-positive S. aureus and 13 mm for gram-negative E. coli. These results demonstrate that Cu-doped ZnO NPs have antibacterial activity, especially against gram-positive bacteria.

The results obtained are supported by previous research demonstrating the improved antibacterial activity of Cu-doped ZnO NPs against gram-positive bacteria relative to gram-negative bacteria (Raghupathi *et al.* 2011; Bhuyan *et al.* 2015; Jung *et al.* 2008). The observed variation in antibacterial activity could potentially be ascribed to structural variations between gram-positive and gram-negative bacteria or an elevated concentration of copper doping. The outer membrane of gram-negative bacteria may lessen the harm caused by Cu-doped ZnO NPs. Furthermore, other reactive oxygen species (ROS) like hydroxyl radicals (OH), singlet oxygen, or superoxide anion (O_2^-) can be produced by Cu-doped ZnO NPs in an aqueous solution, which adds to their antibacterial activity. The direct impact of these negatively charged ROS inside the cell is limited since they are unable to pass through the cell membrane (Lipovsky *et al.* 2005). Zinc ions have the ability to interfere with a variety of bacterial processes at high doses. It affects cellular homeostasis and energy production by inhibiting the breakdown of glucose for energy and by upsetting the proton gradient across the cell membrane. Additionally, it prolongs the lag phase of bacterial development by decreasing the ability of bacteria to thrive in acidic environments. When copper ions bond to DNA molecules, structural alterations are made, which ultimately result in cell death (Hassan *et al.* 2017). Fenton-type reactions can be used by Cu-doped ZnO NPs to stimulate the generation of ROS. Hydrogen peroxide is catalyzed to produce extremely reactive hydroxyl radicals when Cu ions are present. The oxidative stress brought on by the produced ROS can harm bacterial membranes, lipids, proteins, and DNA (Hassan *et al.* 2017). Cell death may result from this damage, which can also cause the cytoplasmic contents to leak out. Overall, both the oxidative damage brought on by ROS production and the direct toxic effects of Zn and Cu ions contribute to the antibacterial activity of Cu-doped ZnO NPs. Their potency against microbiological cells is increased by this dual method. Another possible mechanism by which nanomaterials impact bacterial strains and destroy pathogens is through close interaction between cations (Cu^{2+} and Zn^{2+}) and the negatively charged components of bacterial cell membranes. Further investigation is needed to precisely understand the mechanisms behind the antibacterial activity of Cu-doped ZnO nanoparticles.

Table 3: Inhibition Zone for the ZnO and 1% Cu-ZnO NPs at different amount against E. Coli and Staphylococcus Aureus

Bacteria	ZnO			1% Cu-ZnO		
	250µg	500 µg	1000 µg	250 µg	500 µg	1000 µg
E. Coli (ZOI)						
Streptomycin 100 µg (ZOI-33 mm)	Nil	Nil	12	Nil	Nil	13
Staphylococcus aureus (ZOI)						
Streptomycin 100 µg (ZOI-27mm)	Nil	Nil	Nil	Nil	12	17

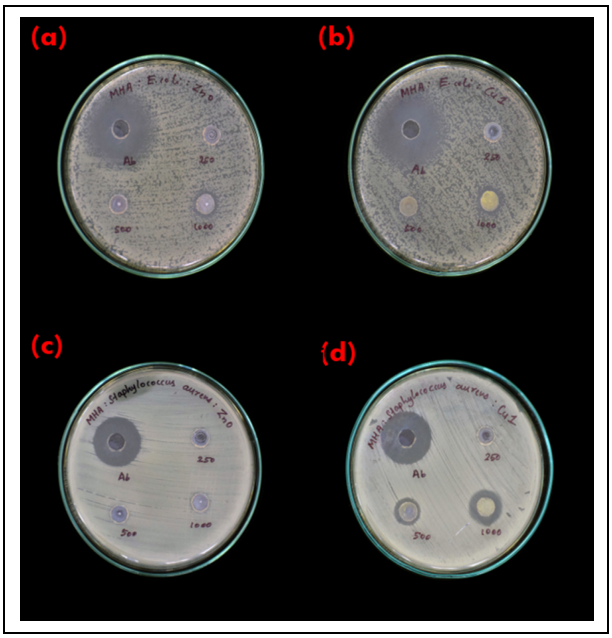

Fig. 10: Photographic images of Zone of Inhibition formed by ZnO NPs (a) and 1% Cu-ZnO NPs (b) against *E. Coli* and by ZnO NPs (c) and 1% Cu-ZnO NPs (d) against *Staphylococcus aureus*

4. CONCLUSION

This work was aimed at the synthesis and characterization of both pure and Cu-doped ZnO nanoparticles at ambient temperature, using a green solvent-mediated solution combustion technique. Plant extract from Moringa oleifera successfully acted as fuel in the synthesis process. Various characterization methods, such as Raman, SEM, EDX, DRS, and XRD were employed to examine the optical and structural characteristics of the nanoparticles. The Cu-doped ZnO nanoparticles had an average crystal size of about 42 nm, as evident from the XRD pattern. The wurtzite hexagonal structure was confirmed to be present in both pure and Cu-doped ZnO nanoparticles by XRD and Raman spectroscopy. Using a Taut plot, the lowering optical band gap of ZnO (3.1 eV) after doping with Cu (2.7 eV) was examined. Evaluation of photocatalytic activity showed that the degradation efficiency for MB dye solution was the highest for Cu-ZnO NPs, reaching about 97%, and the lowest decomposition efficiency was for the pure ZnO NPs (about 20%). The increased photocatalytic and antibacterial capabilities of the Cu-doped ZnO nanoparticles, which were manufactured utilizing Moringa oleifera plant extract as fuel, make them economical, environment-friendly, and potentially useful for wastewater treatment.

ACKNOWLEDGEMENTS

The authors highly acknowledge Center for Research on Molecular Biology and Applied Science, Thiruvananthapuram, India, SAIF MG University, Nirmalagiri College, Koothuparamba, SAIF Cochin, and SAIF MG University, India for providing the characterization facilities.

FUNDING

There is no funding source.

CONFLICT OF INTEREST

The authors declared no conflict of interest in this manuscript regarding publication.

COPYRIGHT

REFERENCES

Ahmad, M., Ahmed, E., Hong, Z. L., Jiao, X. L., Abbas, T. and Khalid, N. R., Enhancement in visible light-responsive photocatalytic activity by embedding Cu-doped ZnO nanoparticles on multi-walled carbon nanotubes, *Appl. Surf. Sci*., 285, 702-712(2013). https://doi.org/10.1016/j.apsusc.2013.08.114

Banu Bahşi, Z. and Oral, A.Y., Effects of Mn and Cu doping on the microstructures and optical properties of sol-gel derived ZnO thin films, *Opt. Mater*., 29(6), 672-678 (2007). https://doi.org/10.1016/j.optmat.2005.11.016

Bhuyan, T., Mishra, K., Khanuja, M., Prasad, R. and Varma, A., Biosynthesis of Zinc oxide nanoparticles from Azadirachtaindica for antibacterial and Photocatalytic applications, *Mater. Sci. Semicond. Process*., 32, 55-61(2015). https://doi.org/10.1016/j.mssp.2014.12.053

Davis, E. A. and Mott, N. F., Conduction in non-crystalline systems V. Conductivity, optical absorption and photoconductivity in amorphous semiconductors, *Phil. Mag.*, 22(179), 903-922(1970). https://doi.org/10.1080/14786437008221061

Deganello, F. and Tyagi, A. K., Solution Combustion Synthesis, Energy and Environment: Best Parameters for Better Materials, *Prog. Cryst. Growth Charact. Mater*., 64(2), 23–61(2018). https://doi.org/10.1016/j.pcrysgrow.2018.03.001

Deka, S. and Joy, P. A., Synthesis and magnetic properties of Mn doped ZnO nanowires, *Solid. State. Commun*., 142, 190–194(2007). https://doi.org/10.1016/j.ssc.2007.02.017

Ding, X., Zhao, K. and Zhang, L, Enhanced Photocatalytic Removal of Sodium Pentachlorophenate with Self-Doped Bi2WO6 under Visible Light by Generating More Superoxide Ions, *Environ. Sci. Technol*., 48(10), 5823-5831(2014). https://doi.org/10.1021/es405714q

Diouri, J., Lascaray, J. P. and El Amrani, M., Effect of the magnetic order on the optical absorption edge in Cd1−xMnxTe, *Phys. Rev. B*., 31(12), 7995(1985). https://doi.org/10.1021/es405714q

Geetha, D. and Thilagavathi, T., Hydrothermal Synthesis of Nano ZnO Structures from CTAB, Dig. *J. Nanomater. Bios*., 5(2), 297-301 (2010).

Hassan, I. A. and others., Antimicrobial properties of copper doped ZnO coatings under darkness and white light illumination. *ACS. Omega.*, 2(8), 4556-4562 (2017). https://doi.org/10.1021/acsomega.7b00759

He, J. H., Lao, C. S., Chen, L. J., Davidovic, D. and Wang, Z. L, Large-Scale Ni-Doped ZnO Nanowire Arrays and Electrical and Optical Properties, *J. Am. Chem. Soc.*, 127(47), 16376-16377(2005). https://doi.org/10.1021/ja0559193

Hyun, K., J., Kim, H., Kim, D., Ihm, Y. and Kil Choo, W., The origin of room temperature ferromagnetism in cobalt-doped zinc oxide thin films fabricated by PLD, *J. Eur. Ceram. Soc*., 24(6), 1847-1851 (2004). https://doi.org/10.1016/S0955-2219(03)00447-3

Jung, W. K., Koo, H. C., Kim, K. W., Shin, S., Kim, S. H. and Park, Y. H., Antibacterial activity and mechanism of action of the silver ion in staphylococcus aureus and Escherichia coli, *Appl. Environ. Microbiol*., 74(7), 2171-2178 (2008). https://doi.org/10.1128/AEM.02001-07

Labhane, P. K., Huse, V. R., Patle, L. B., Chaudhari, A. L. and Sonawane, G. H., Synthesis of Cu doped ZnO nanoparticles: crystallographic, optical, FTIR, morphological and photocatalytic study, *J. Chem. Eng*., 03(07), 39-51 (2015). https://doi.org/10.4236/msce.2015.37005

Lipovsky, A. and others., EPR Study of visible light-induced ROS generation by nanoparticles of ZnO, *J. Phys. Chem. C*, 113(36), 15997-16001 (2009). https://doi.org/10.1021/jp904864g

Lupan, O., Chow, L., Ono, L. K., Roldan Cuenya, B., Chai, G., Khallaf, H., Park, S. and Schulte, A.,. Synthesis and characterization of Ag- or Sb-doped ZnO nanorods by a facile hydrothermal route, *J. Phys. Chem. C*., 114, 12401-12408 (2010). https://doi.org/10.1021/jp910263n

Mahajan, B. K., Kumar, N., Chauhan, R., Srivastava,V. C. and Gulati, S., Mechanistic evaluation of heterocyclic aromatic compounds mineralization by a Cu doped ZnO photo-catalyst, *Photochem. Photobiol. Sci*., 18(6), 1540-1555 (2019). https://doi.org/10.1039/C8PP00580J

Manju, K., Micro-Raman investigation of nano-crystalline ZnO and ZnO doped with Al, *RP Current Trends in Eng. Tech*.,1(3), 57–61 (2022). https://doi.org/10.1016/j.heliyon.2024.e26401

Menon, S., Rajeshkumar, S. and Venkat Kumar, S., A review on biogenic synthesis of gold nanoparticles, characterization, and its applications, *Resour. Effic. Technol*., 3(4), 516-527(2017). https://doi.org/10.1016/j.reffit.2017.08.002

Mo, Z., Huang, Y., Lu, S., Fu, Y., Shen, X. and He, H., Growth of ZnO nanowires and their applications for CdS quantum dots sensitized solar cells, *Optik*,149, 63-68(2017). https://doi.org/10.1016/j.ijleo.2017.09.035

Mhamdi, A., Mimouni, R., Amlouk, A., Amlouk, M. and Belgacem, S, Study of copper doping effects on structural, optical and electrical properties of sprayed ZnO thin films, *J. Alloys. Comp*., 610, 250(2014). https://doi.org/10.1016/j.jallcom.2014.04.007

Mott, N. F. and Davis, E. A., Conduction processes in non-crystalline materials, *Oxford. Clarendon Press*., (1971).

Muthukumaran, S. and Gopalakrishnan, R., Structural, FTIR and photoluminescence studies of Cu doped ZnO nanopowders by co-precipitation method, *Opt. Mater*., 34(11), 1946-1953(2012). https://doi.org/10.1016/j.optmat.2012.06.004

Nimbalkar, A. R. and Patil, M. G., Synthesis of highly selective and Sensitive Cu doped ZnO think film sensor for detection of H2S gas, *Mater. Sci. Semicond. Process*., 71, 332-341(2017). https://doi.org/10.1016/j.mssp.2017.08.022

Ozgur, U., Alivov, Y. I., Liu, C., Teke, A., Reshchikov, M. A., Doğan, S., Avrutin, V., Cho, S. J. and Morkoç, H., A comprehensive review of ZnO materials and devices, *J. Appl. Phys*., 98(4), 41-301(2005). https://doi.org/10.1063/1.1992666

Pandian, L., Rajasekaran, R. and Govindan, P., Synthesis, characterization and application of Cu doped ZnOnanocatalys for photocatalytic ozonation of textile dye and study of its reusability. *Mater. Res. Express*., 5, 115-505(2018). https://doi.org/10.1088/2053-1591/aadcdf

Premanathan, M., Karthikeyan, K., Jeyasubramanian. and Manivannan, K., Selective, G., toxicity of ZnO nanoparticles toward gram positive bacteria and cancer cells by apoptosis through lipid peroxidation. *Nanomed*., 7(2), 184-192(2011). https://doi.org/10.1016/j.nano.2010.10.001

Qi, D., Xing, M. and Zhang, J., Hydrophobic Carbon-Doped TiO2/MCF-F Composite as a High Performance Photocatalyst, *J. Phys. Chem. C*., 118(14), 7329–7336(2014). https://doi.org/10.1021/jp4123979

Qiu, B., Xing, M. and Zhang, J., Nanocrystals Grown in Situ on Graphene Aerogels for High Photocatalysis and Lithium-Ion Batteries, *J. Am. Chem. Soc*., 136(16), 5852–5855(2014). https://doi.org/10.1021/ja500873u

Raghupathi, K. R., Koodali, R. T. and Manna, A. C., Size- Dependent bacterial growth inhibition and mechanism of antibacterial activity of Zinc Oxide nanoparticles, *Langmuir*., 27(7), 4020-4028(2011). https://doi.org/10.1021/la104825u

Ravichandran, K., Mohan, R., Sakthivel, B., Varadharajaperumal, S., Devendran, P., Alagesan, T. and Pandian, K., Enhancing the photocatalytic efficiency of sprayed ZnO thin films through double doping (Sn + F) and annealing under different ambiences, *App. Surf. Sci*., 321, 310–317(2014). https://doi.org/10.1016/j.apsusc.2014.10.023

Richa, B., Amardeep, B., Jitendra, P. S., Keun, H. C., Navdeep, G. and Sanjeev, G., Structural and Electronic Investigation of ZnO Nanostructures Synthesized under Different Environments, *Heliyon*, 4(4), E00594(2018). https://doi.org/10.1016/j.heliyon.2018.e00594

Saleh, R., N. and Djaja, F., Transition-metal-doped ZnO nanoparticles: Synthesis, characterization and photocatalytic activity under UV light, Spectrochim, *Acta. A. Mol. Biomol. Spectrosc*., 130, 581–590 (2014). https://doi.org/10.1016/j.saa.2014.03.089.

Shikha, Y., Shreya, and Peeyush, P., Hydrothermal synthesis and characterization of tin telluride, *RP. Current. Trends. In. Appl. Sci*., 3(1), 14–19(2024).

Singhal, S., Kaur, J., Namgyal, T. and Sharma, R., Cu-Doped ZnO Nanoparticles: Synthesis, Structural and Electrical Properties, *Phys. B. Condens. Matter*., 407(8), 1223-1226(2012). https://doi.org/10.1016/j.physb.2012.01.103

Silambarasan, M., Saravanan, S. and Soga, T., Raman, and Photoluminescence Studies of Ag and Fe-doped ZnO Nanoparticles, *Int. J. ChemTech Res*., 7(3), 1644-1650(2015).

Taut, J., Grigorovici, R. and Vancu, A., Optical properties and electronic structure of amorphous germanium, *Phys. Status. Solidi.*,15, 627-637(1966). https://doi.org/10.1002/pssb.19660150224

Thilagavathi, T. and Geetha, D., Nano ZnO Structures Synthesized in Presence of Anionic and Cationic Surfactant under Hydrothermal Process, *Appl. Nanosci*., 4, 127-132(2014). https://doi.org/10.1007/s13204-012-0183-8

Wang, Y., Xu, M., Li, J., Ma, J., Wang, X., Wei, Z., Chu, X., Fang, X. and Jin, F., Nb and Ta Co-Doped TiO_2 Transparent Conductive Thin Films by Magnetron Sputtering: Fabrication, Structure, and Characteristics, *J. Elect. Mater*., 9, 5334-5343(2018). https://doi.org/10.5772/63234

Wibowo, J. A. and others., Cu- and Ni-Doping Effect on Structure and Magnetic Properties of Fe-Doped ZnO Nanoparticles, *Adv. Mater. Phy. Chem*., 3(01), 48-57 (2013). https://doi.org/10.4236/ampc.2013.31008

Xing, M., Fang, W., Yang, X., Tian, B. and Zhang, J., Highly-dispersed boron-doped graphene nanoribbons with enhanced conductibility and photocatalysis, *Chem. Commun*., 50, 6637-6640(2014). https://doi.org/10.1039/C4CC01341G

Zhang, S., Li, J., Zeng, M., Li, J., Xu, J. and Wang, X., Bandgap Engineering and Mechanism Study of Nonmetal and Metal Ion Co-doped Carbon Nitride: C+Fe as an Example, *Chem. Eur. J*., 20(31), 9805–9812(2014). https://doi.org/10.1002/chem.201400060

Zhou, X. S., Zhao, C., Hou, R., Zhang, J., Kirk, K. J., Hutson, D., Guo, Y. J., Hu, P. A., Peng, S. M., Zu, X. T. and Fu, Y. Q., Sputtered ZnO film on aluminium foils for flexible ultrasonic transducers, *Ultrasonics*, 54(7), 1991-1998(2014). https://doi.org/10.1016/j.ultras.2014.05.006